

RESEARCH ARTICLE

Active Notch signaling is required for arm regeneration in a brittle star

Vladimir Mashanov^{1,2*}, Jennifer Akiona¹, Maleana Khoury¹, Jacob Ferrier³, Robert Reid³, Denis Jacob Machado³, Olga Zueva¹, Daniel Janies³**1** Department of Biology, University of North Florida, Jacksonville, FL, United states of America, **2** Wake Forest Institute for Regenerative Medicine, Winston Salem, NC, United states of America, **3** University of North Carolina at Charlotte, Charlotte, NC, United states of America* vmashano@wakehealth.edu

OPEN ACCESS

Citation: Mashanov V, Akiona J, Khoury M, Ferrier J, Reid R, Machado DJ, et al. (2020) Active Notch signaling is required for arm regeneration in a brittle star. PLoS ONE 15(5): e0232981. <https://doi.org/10.1371/journal.pone.0232981>**Editor:** Thomas A Reh, University of Washington, UNITED STATES**Received:** December 7, 2019**Accepted:** April 24, 2020**Published:** May 12, 2020**Copyright:** © 2020 Mashanov et al. This is an open access article distributed under the terms of the [Creative Commons Attribution License](https://creativecommons.org/licenses/by/4.0/), which permits unrestricted use, distribution, and reproduction in any medium, provided the original author and source are credited.**Data Availability Statement:** All datasets were deposited to NCBI's Gene Expression Omnibus (GSE142391, <https://www.ncbi.nlm.nih.gov/geo/query/acc.cgi?acc=GSE142391>).**Funding:** Research reported in this publication was supported by The National Institute of General Medical Sciences of the National Institutes of Health under award number R15GM128066. University of North Florida and The University of North Carolina at Charlotte (College of Computing and Informatics, The University Honors Program, The University Professional Internship Program,

Abstract

Cell signaling pathways play key roles in coordinating cellular events in development. The Notch signaling pathway is highly conserved across all multicellular animals and is known to coordinate a multitude of diverse cellular events, including proliferation, differentiation, fate specification, and cell death. Specific functions of the pathway are, however, highly context-dependent and are not well characterized in post-traumatic regeneration. Here, we use a small-molecule inhibitor of the pathway (DAPT) to demonstrate that Notch signaling is required for proper arm regeneration in the brittle star *Ophioderma brevispina*, a highly regenerative member of the phylum Echinodermata. We also employ a transcriptome-wide gene expression analysis (RNA-seq) to characterize the downstream genes controlled by the Notch pathway in the brittle star regeneration. We demonstrate that arm regeneration involves an extensive cross-talk between the Notch pathway and other cell signaling pathways. In the regrowing arm, Notch regulates the composition of the extracellular matrix, cell migration, proliferation, and apoptosis, as well as components of the innate immune response. We also show for the first time that Notch signaling regulates the activity of several transposable elements. Our data also suggests that one of the possible mechanisms through which Notch sustains its activity in the regenerating tissues is via suppression of Neuralized1.

Introduction

In metazoans, a surprisingly small number of signaling pathways are required to control animal development [1]. Knowledge of how these pathways work and interact in different contexts is key to gaining a mechanistic understanding of processes, including development, growth and post-traumatic regeneration in adults. Post-traumatic regeneration often requires dynamic changes in the balance between undifferentiated progenitors and specialized differentiated cells. In response to trauma, the cells of the damaged adult tissue have to be activated and instructed to re-enter the cell cycle, engage in migratory behavior with coordinated spatial rearrangements, and eventually differentiate into specialized cell types of a new body part. As

The Department of Bioinformatics and Genomics, and the University Research Computing division) 25% (\$101,313.54) of the project was funded with Federal money. There was no funding from nongovernmental sources. The funders had no role in study design, data collection and analysis, decision to publish, or preparation of the manuscript. The content is solely the responsibility of the authors and does not necessarily represent the official views of the National Institutes of Health.

Competing interests: The authors have declared that no competing interests exist.

regeneration progresses, most of the newly generated cells have to stop dividing and migrating to differentiate into specialized cell types or enter a quiescent state. A proportion of the cells are spared from terminal differentiation to be able to serve as a source of new cells for normal cell turnover and/or for future regeneration events. Therefore, regeneration requires complex changes in cell dynamics, which must be tightly coordinated in space and time by genetically encoded signaling pathways.

The genes encoding for the Notch signaling pathway are highly conserved in the animal kingdom [1–4]. This pathway regulates various key cellular events including: differentiation, fate specification, proliferation, death, and patterning into tissues [2–8]. The functional role of Notch signaling has been extensively characterized in both vertebrate and invertebrate embryos, as well as in adult tissues that undergo dynamic cell turnover. Functions of the Notch signaling are very diverse, context-dependent, and often even opposing. Depending on the particular organisms and the tissue, Notch can either promote cell differentiation or facilitate stem cell maintenance, suppress or facilitate cancer progression, induce synthesis or degradation of the extracellular matrix components [5, 8].

The Notch signaling pathway works through a juxtacrine mechanism. Both Notch ligands (on the signaling cell) and receptors (on the target cell) are integrated transmembrane proteins. Thus direct contact between two cells is required for a signaling event to occur. Upon binding to its ligand, the Notch receptor undergoes conformational changes, which expose a cleavage site for the enzyme γ -secretase. This enzyme releases the Notch intracellular domain (NICD) from its connection to the plasma membrane. The NICD is then transported to the nucleus, where it activates the CSL transcription factors and thus initiates the expression of several other downstream transcription factors, including Hes, Hey, Snail, as well as cyclins, and other genes [9, 10]. Since the proteolytic cleavage of the Notch receptor plays a crucial role in the function of the signaling pathway, targeting the γ -secretase activity with small-molecule inhibitors, such as DAPT, has become a commonly used strategy to study the pathway.

Even though Notch signaling has been studied extensively in the context of embryonic development, cancer, and stem cell function, much less is known about the role(s) that this pathway plays in post-traumatic regeneration. The available data suggests that the Notch signaling is essential for regeneration in several model organisms. For example, it has been shown that Notch is required for proper head and tentacle regeneration in *Hydra* [11], control of cell differentiation during retinal regeneration in newts [12], regulation of cardiomyocyte proliferation in zebrafish heart regeneration [13], and whole-body regeneration in planarians [14]. However, much less is known about the function of the pathway in other regenerative species.

Echinoderms are a phylum of multicellular invertebrates with highly regenerative species that can regrow almost all tissue types and share a deep common ancestor with chordates. These features make echinoderms particularly attractive model organisms in regenerative biology [15, 16]. However, the molecular events that drive echinoderm regeneration, including the functional role(s) of the critical signaling pathways, are still poorly understood at the mechanistic level. Genes encoding all major components of the Notch pathway are present in echinoderms. They have been first identified in the fully sequenced genome of the sea urchin *Strongylocentrotus purpuratus* (Stimpson, 1857) [5]. Similarly, our earlier data from the transcriptomic analysis showed that key members of the Notch signaling pathway were expressed in both the uninjured and regenerating radial nerve cord of the sea cucumber *Holothuria (Selenkothuria) glaberrima* Selenka, 1867 [17]. These genes include the Notch receptor, ligands (Delta and Serrate), the transcriptional regulator RBPJ, two Notch target genes of the Hes family, and the Notch signaling modulator Numb. The only context, in which expression of those genes was studied at the cell and tissue levels in echinoderms, was sea urchin embryogenesis

[18, 19]. The only functional study of the Notch signaling pathway in the context of adult echinoderm regeneration was performed in the sea urchin *Lytechinus variegatus* [20]. This work demonstrated the requirement of the functional Notch signaling for the proper outgrowth of amputated external appendages, such as spines and podia. The cellular and molecular processes regulated by Notch signaling in echinoderm regeneration remain unknown. In addition, echinoid spines and podia are relatively simple structures. The role of the Notch signaling pathway in the regeneration of more complex organ systems and appendages in adult echinoderms has yet to be addressed.

Our aim in this study is to establish the functional role of the Notch signaling in arm regeneration in the brittle star *Ophioderma brevispina* (Say, 1825) and identify the target genes that are regulated by the pathway. Brittle star arms are segmented body appendages with complex internal anatomy. Each brittle star arm contains a calcareous endoskeleton composed of serial vertebral ossicles and several peripheral elements. Associated with the skeleton, the brittle star arm has a system of muscles and ligaments, two systems of coelomic canals, and a complex nervous system including a radial nerve and numerous peripheral nerves [21, 22]. Brittle stars have emerged as important models in regenerative biology. They have been used in studies of skeletogenesis and biomineralization [23, 24], morphogenesis, and regulation of growth and differentiation [25]. Here, we show that exposing regenerating brittle stars to the Notch pathway antagonist DAPT significantly impairs regeneration. We also identified genes regulated, directly or indirectly, by the pathway by performing a transcriptome-wide gene expression analysis (RNA-Seq). We show that Notch affects a multitude of biological processes involved in arm regeneration, including the extracellular matrix composition and remodeling, cell proliferation, death and migration, activity of mobile genetic elements, and the innate immune response. Our data also indicates an extensive cross-talk between Notch signaling and other key cell signaling pathways, such as Wnt, TGF- β , Toll, JNK, and others, suggesting that regeneration depends on a complex regulatory environment.

Results

The Notch signaling pathway in the brittle star

As expected, genes corresponding to the major components of the Notch pathway (i.e., the Notch receptor, the Delta and Serrate ligands, the transcriptional regulator RBPJ, two Notch target genes of the Hes family, and the Notch signaling modulator), as well as a Notchless protein homolog that plays a role in the Notch signaling pathway, were identified in the complete transcriptome of *O. brevispina*. Details are provided on a general Feature Format version 3 (GFF3) file, available in the supplements to this article (S1 File).

Pharmacological inhibition of the Notch signaling slows down arm regeneration

On day 14 post-autotomy, after continuous exposure of the treatment and control cohorts to the DAPT reagent (3 μ M) or DMSO (vehicle), respectively, two arms from each individual were processed for histological analysis. Six individuals per experimental group were used. As compared to the control individuals, the length of the regenerated arm (outgrowth) in the DAPT-treated cohort was on average 37% shorter (967 μ m vs 605 μ m, T-test p -value = 0.002) (Figs 1 and 2A). Likewise, the newly regenerated arm portion in the DAPT-treated animals had, on average, two fewer segments than the arms in the control group (5.5 vs 7.5, T-test p -value = 0.047) (Fig 2B). Even though the new arms in the DAPT-treated individuals were smaller and less segmented, they still contained all major radial organs, including the radial

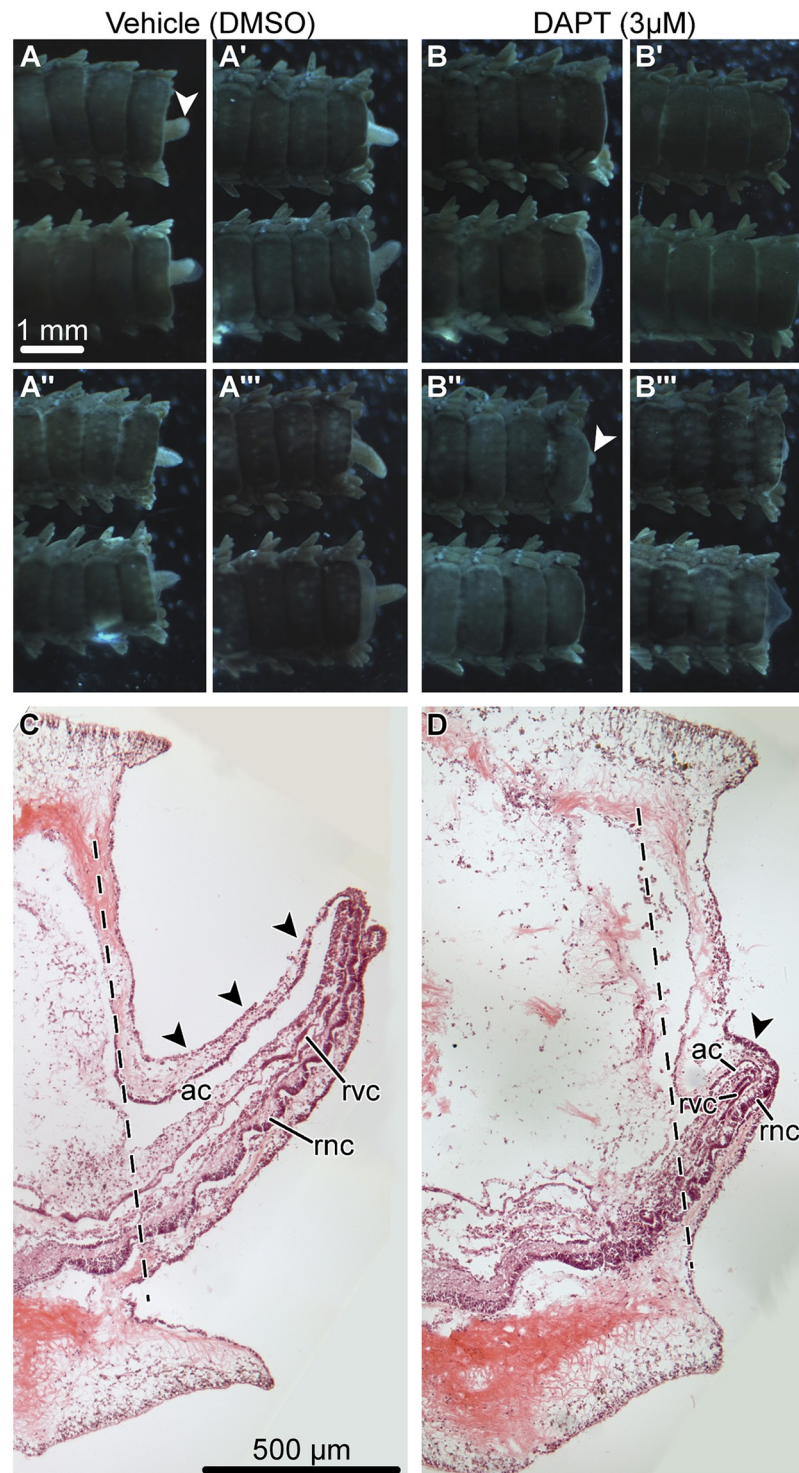


Fig 1. Effect of DAPT (3 μ M) treatment on the structure of the regenerating arm (day 14 post-autotomy). A—A''': Aboral view of regenerating arms from four representative control animals exposed to DMSO (vehicle). Two arms from each animal are shown. B—B''': Aboral view of regenerating arms from four representative animals exposed to 3 μ M DAPT. Two arms from each animal are shown. C and D: Representative sagittal sections through the regenerating arm of a control (DMSO-treated) individual (C) and a DAPT-treated individual (D). Hematoxylin and eosin staining. Arrowheads show the arm outgrowth (regenerate). Dashed lines show the position of the autotomy plane. Abbreviations: *ac*—arm coelom; *rnc*—radial nerve cord; *rvc*—radial canal of the water-vascular system.

<https://doi.org/10.1371/journal.pone.0232981.g001>

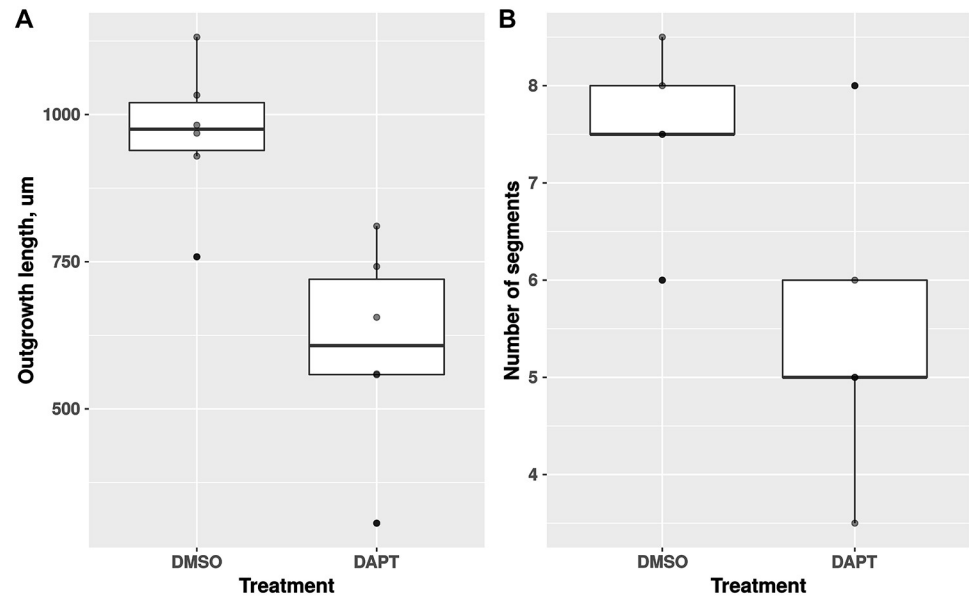


Fig 2. Boxplots showing the effect of DAPT (3 μ M) treatment on the length of the outgrowth (A) and the number of segments in the regenerating arm (B). By day 14 post-autotomy, the DAPT treatment significantly reduced both the total length of the outgrowth (by the factor of 1.6, T-test p -value = 0.002) and the number of segments in the new arm (by the factor of 1.4, T-test p -value = 0.047).

<https://doi.org/10.1371/journal.pone.0232981.g002>

nerve cord, the radial canal of the water-vascular system, and the arm coelom (compare Fig 1C and 1D).

***De novo* transcriptome assembly**

We are generating genomic and transcriptomic resources for the brittle star *O. brevispina*. However, since at the time of writing the assembly and annotation of the full genome for this species is still in preparation, we chose to use a *de novo* assembled transcriptome as a reference to characterize the Notch pathway target genes.

The *de novo* transcriptome was generated from 17,318,775 MiSeq and 832,245,006 HiSeq quality filtered and adapter trimmed reads. The single MiSeq library represented pooled samples from intact and regenerating arms at different states of regeneration, whereas six HiSeq libraries corresponded to three control (DMSO-treated) and three DAPT-treated regenerating individuals on day 14 post-autotomy (see Methods). Sequence reads were assembled with Trinity [26, 27] into 2,463,269 contigs (1,169,021 Trinity “genes”) with the average/median contig length of 421.6/260 nt and contig N50 of 527 nt. The key assembly metrics are listed in Table 1.

To assess the quality of the assembled transcriptome, we performed a series of benchmark tests. First, to assess the representation of reads in the transcriptome, all cleaned Illumina reads were aligned back to the assembled contigs with Bowtie 2 [28]. The vast majority of the reads (94.09%) mapped back to the assembly. Of these, 75.42% of the reads aligned as proper pairs one (21.62%) or more (53.80%) times.

Second, to determine the representation of completely or almost completely (>80% of the length) assembled protein-coding transcripts, we compared our contigs to the reference proteome of the sea urchin *S. purpuratus* [29], the echinoderm species with the best-annotated

Table 1. Key metrics of the *de novo* assembly.

Metric	Value
Total assembled bases	1,038,536,368 nt
Number of contigs	2,463,269
Number of Trinity “genes”	1,169,021
Shortest contig	151 nt
Longest contig	48,146 nt
Average contig length	421.6 nt
Median contig length	260 nt
Contig N50	527 nt
Overall read alignment rate	94.09%
Reads aligned as proper pairs	75.42%
Full-length transcript representation	7,397 (out of 35,786)
Complete (single-copy/duplicated) BUSCOs	98.7% (28.8%/69.9%)

<https://doi.org/10.1371/journal.pone.0232981.t001>

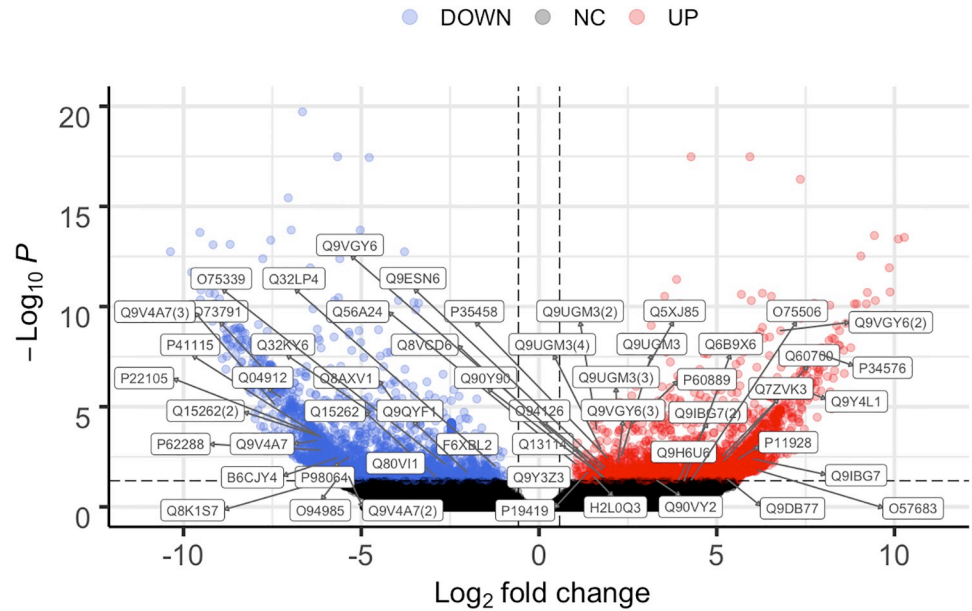
genome to date. This analysis showed that 7,397 sea urchin orthologs (out of 35,786) are represented in our transcriptome by full-length and nearly full-length transcripts.

Third, the completeness of the assembly in terms of protein-coding gene content was assessed using BUSCO [30] and the conserved metazoan gene dataset. Out of 978 genes (or 98.7%) in the metazoan database, 966 genes were recovered in the assembled transcriptome as “complete” (i.e., their length fell within two standard deviations of the BUSCO group mean length). Of these complete genes, 282 matched a single contig, whereas multiple copies represented the remaining 684. The high number of “duplicated” genes is a known phenomenon in *de novo* transcriptome assembly, as even in the absence of any sequencing errors, inherent biological complexity of the transcriptome (e.g., single nucleotide polymorphism and alternative splicing) makes assembly algorithms report multiple isoforms for individual genes [31].

Identification of the genes affected by the Notch pathway perturbation

To identify genes, whose expression changes in response to the Notch signalling perturbation, we performed a transcriptome-wide gene expression comparison between the DAPT-treated cohort and the control (vehicle-treated) animals. These differentially expressed genes comprise potential direct and indirect targets of the pathway. To reduce the redundancy of the *de novo* assembled transcriptome and to be able to perform transcript expression quantification at the “gene” level, we clustered the 2,463,269 Trinity contigs into 1,012,954 “clusters” using the Corset tool [32]. Corset was applied after the reads representing the libraries from the control and DAPT-treated individuals were aligned back to the assembled transcriptome [33]. Differential gene expression analysis was performed with the DESeq2 package [34], which identified 1,978 significantly up-regulated transcripts and 2,434 significantly down-regulated in the DAPT-treated cohort, as compared to control (DMSO-treated) individuals. For the purposes of this study, differentially expressed genes were defined as those whose expression in response to DAPT treatment changed by at least the factor of 1.5 in either direction and the associated *p*-value of the statistical test adjusted for multiple comparisons was less than 0.05 (Fig 3).

To extract the biological meaning behind these extensive lists of genes, we used the DAVID functional annotation resource [35, 36]. We annotated the transcripts representing the Corset clusters by comparing them against the Uniprot database. This approach yielded lists of Uniprot IDs for up- and down-regulated genes, containing 180 and 142 entries, respectively. As the “gene population background” [35], we used a list of 59,110 entries yielded by annotation



Total = 970598 variables

Fig 3. Differentially expressed genes in the DAPT-treated animals as compared to the control (DMSO-treated) cohort. Volcano plot showing the log₂ fold change on the X-axis and -log₁₀ of adjusted p-values on the Y-axis. The significantly up-regulated transcripts (red) are to the right, and significantly down-regulated transcripts (blue) are to the left. Each gene is represented with a dot. Grey dots represent the genes whose expression level did not change significantly in response to DAPT treatment. The differentially expressed contigs were defined as those whose associated adjusted p-value was less than 0.05 and the log₂ fold change in expression exceeded ±0.58. Volcano plot showing the log₂ fold change on the X-axis and -log₁₀ of adjusted p-values on the Y-axis. Each gene is represented with a dot. The 1,978 significantly up-regulated transcripts (red) are to the right, and the 2,434 significantly down-regulated transcripts (blue) are to the left. Grey dots represent the genes whose expression level did not change significantly in response to DAPT treatment. The differentially expressed contigs were defined as those whose associated adjusted p-value was less than 0.05 and the log₂ fold change in expression exceeded ±0.58. Boxed labels represent UniProt IDs (with label copy number within parenthesis) shown in Tables 2 and 3.

<https://doi.org/10.1371/journal.pone.0232981.g003>

of all Corset clusters. The percentage of the gene identifiers that were successfully “mapped” to the internal IDs within the DAVID knowledge base were 89%, 88%, and 92% for the list of down-regulated, up-regulated and “background” genes, respectively. In DAVID, we then used the “mapped” genes to perform functional annotation clustering by classifying the input genes into groups based on measuring relationships among annotation terms associated with these genes. Each cluster is assigned an enrichment score, which is defined as the geometric mean of the enrichment p-values associated with each annotation term in the group [35]. The results of the DAVID cluster analysis are shown in Tables 2 and 3. The few genes, whose identifiers failed to map to the DAVID database, were annotated manually (Tables 4 and 5).

The down-regulated genes clustered by DAVID include genes that (a) code for extracellular matrix proteins and mediate interactions between cells and the extracellular matrix (e.g., cell adhesion), (b) regulation of multiple signaling pathways (including TGF-β, retinoic acid, JNK, p38, NF-kappa-B, JUN, TNF, Wnt, Toll-like receptor signaling, and EFGR signaling), (c) innate immune response (antiviral response, phagocytosis, lectin pathway), (d) protein ubiquitination involved in protein homeostasis, quality control, immunity, cell death, and regulation of cell signaling transduction, (e) cell survival, proliferation, and differentiation; (f) semaphorin signaling, cytoskeleton organization/remodeling and cell migration, (g) function of the endomembrane system, including the endoplasmic reticulum; (h) cellular homeostasis,

Table 2. DAVID functional clustering of down-regulated genes.

Annotation Cluster	Representative Annotation Term	Enrichment score	Representative Ortholog	UniprotID	Log ₂ Fold Change
1	GO:0005578 ~ proteinaceous extracellular matrix	1.27	Tenascin-X	P22105	-6.33
2	GO:0009628 ~ response to abiotic stimulus	1.24	Receptor-type tyrosine-protein phosphatase kappa	Q15262	-6.25
3	GO:0005576 ~ extracellular region	1.00	Cartilage intermediate layer protein 1	O75339	-2.65
4	GO:0004842 ~ ubiquitin-protein transferase activity	1.00	E3 ubiquitin-protein ligase TRIM56	Q80VI1	-3.34
5	GO:0006955 ~ immune response	0.90	Mannan-binding lectin serine protease 1	P98064	-5.36
6	GO:1902287 ~ semaphorin-plexin signaling pathway involved in axon guidance	0.67	Plexin-B	Q9V4A7	-7.44
7	GO:0007166 ~ cell surface receptor signaling pathway	0.53	Kremen protein 2	Q8K1S7	-5.53
8	GO:0007010 ~ cytoskeleton organization	0.27	Abnormal spindle-like microcephaly-associated protein homolog	P62288	-6.16
9	GO:0016567 ~ protein ubiquitination	0.24	TNF receptor-associated factor 6	B6CJY4	-5.68
10	GO:0005783 ~ endoplasmic reticulum	0.20	Retinol dehydrogenase 11	Q9QYF1	-2.03
11	GO:0006873 ~ cellular ion homeostasis	0.19	Sodium-driven chloride bicarbonate exchanger	Q32LP4	-1.24
12	GO:0009653 ~ anatomical structure morphogenesis	0.18	Tyrosine-protein kinase receptor Tie-2	O73791	-7.24
13	GO:0006468 ~ protein phosphorylation	0.14	Macrophage-stimulating protein receptor	Q04912	-7.27
14	GO:0005840 ~ ribosome	0.11	40S ribosomal protein S11	P41115	-6.12
15	GO:0051641 ~ cellular localization	0.08	Endophilin-A1	Q8AXV1	-3.93
16	GO:1901265 ~ nucleoside phosphate binding	0.05	dCTP pyrophosphatase 1	Q32KY6	-4.74
17	GO:0012505 ~ endomembrane system	0.02	Calsyntenin-1	O94985	-5.7
18	GO:0044237 ~ cellular metabolic process	0.01	26S proteasome non-ATPase regulatory subunit 11	F6XBL2	-1.73

<https://doi.org/10.1371/journal.pone.0232981.t002>

including regulation of intracellular ion concentration and ribosomal structure and function (Table 2).

Out of 14 down-regulated genes that did not get mapped to the DAVID database, seven represented proteins derived from retrotransposon genes (e.g., DNA-polymerase, reverse transcriptase, Pol). The remaining genes encode for three lectins, an antibacterial protein neuro-macin and the antiviral tripartite motif-containing protein 5 (Table 4).

The up-regulated genes in DAVID functional clusters are known to be involved in (a) innate immune activity (antiviral and antibacterial), (b) cell signaling pathways (Toll-like, NF-kappa-B, JNK, p38, MAPK, VEGF, TOR, TGF-beta, BMP, Wnt), (c) positive regulation of neuronal and synaptic differentiation; (d) cell proliferation and differentiation; (e) cell death and removal of apoptotic cells by phagocytosis; (f) stress response (e.g., hypoxia, mitochondrial stress, negative regulation of the heat shock response); (g) epigenetic regulation (e.g., maintaining the transcriptionally repressing state by Polycomb proteins), (f) cell adhesion and migration; (g) RNA maturation, processing and splicing, (h) mitochondrial function in cellular respiration and cell death (Table 3). One of the genes that are up-regulated in response to inhibition of the Notch pathway is E3 ubiquitin-protein ligase Neurl1, an inhibitor of the Notch pathway, suggesting a control mechanism through mutual inhibition.

Among 18 up-regulated genes that did not have a match in the DAVID database, seven represented transcripts derived from transposable elements, including a transposase from a Tc3-like DNA transposon, reverse transcriptase genes from three retroelements, and two putative retrotransposon integrase genes. The remaining unmapped genes are involved in innate immune response, cell signaling, cell adhesion, lipoprotein endocytosis, amino acid

Table 3. DAVID functional clustering of up-regulated genes.

Annotation Cluster	Representative Annotation Term	Enrichment score	Representative Ortholog	UniprotID	Log ₂ Fold Change
1	GO:0002376 ~ immune system process	1.49	Deleted in malignant brain tumors 1 protein	Q9UGM3	2.19
2	GO:0002682 ~ regulation of immune system process	1.18	TNF receptor-associated factor 3	Q13114	1.76
3	GO:0010941 ~ regulation of cell death	1.08	Cell death specification protein 2	Q94126	1.78
4	PF13445:RING-type zinc-finger	0.84	Tripartite motif-containing protein 2	Q9ESN6	1.83
5	GO:0080134 ~ regulation of response to stress	0.77	Heat shock factor-binding protein 1	O75506	4.29
6	GO:0007154 ~ cell communication	0.74	Mitogen-activated protein kinase 12 Map3k12	60700	v6.03
7	GO:0048856 ~ anatomical structure development	0.71	Myeloid differentiation primary response protein MyD88	Q5XJ85	2.73
8	GO:0004842 ~ ubiquitin-protein transferase activity	0.69	Kelch-like protein 24	Q56A24	1.04
9	GO:0004871 ~ signal transducer activity	0.68	Gamma-aminobutyric acid type B receptor subunit 1	H2L0Q3	1.53
10	GO:0005576 ~ extracellular region	0.65	Kielin/chordin-like protein	Q9IBG7	6.05
11	GO:0006163 ~ purine nucleotide metabolic process	0.64	2'-5'-oligoadenylate synthase 1A	P11928	5.61
12	GO:0080134 ~ regulation of response to stress	0.61	Hypoxia up-regulated protein 1	Q9Y4L1	7.17
13	PF00431:CUB domain	0.58	Kremen protein 1	Q90Y90	1.82
14	GO:0016021 ~ integral component of membrane	0.46	Tumor necrosis factor receptor superfamily member EDAR	Q90VY2	3.32
15	GO:0007010 ~ cytoskeleton organization	0.45	Dynactin subunit 1	P35458	1.92
16	GO:0045944 ~ positive regulation of transcription from RNA polymerase II promoter	0.40	ETS domain-containing protein Elk-1	P19419	1.37
17	GO:0017076 ~ purine nucleotide binding	0.32	Deoxynucleoside triphosphate triphosphohydrolase SAMHD1	Q9Y3Z3	1.06
18	GO:0071944 ~ cell periphery	0.29	Transmembrane cell adhesion receptor mua-3	P34576	7.91
19	GO:0044430 ~ cytoskeletal part	0.21	Protein Skeletor	Q9VGY6	6.80
20	GO:0051246 ~ regulation of protein metabolic process	0.21	NAD-dependent protein deacetylase sirtuin-2	Q7ZVK3	5.17
21	GO:0006468 ~ protein phosphorylation	0.19	Alpha-protein kinase vwkA	Q6B9X6	4.09
22	GO:0032991 ~ macro-molecular complex	0.17	Splicing factor 3B subunit 1	O57683	6.15
23	GO:0044281 ~ small molecule metabolic process	0.14	Elongation of very long chain fatty acids protein 4	Q3S8M	2.00
24	GO:0044085 ~ cellular component biogenesis	0.09	Breast carcinoma-amplified sequence 3	Q9H6U6	2.89
25	GO:0005783 ~ endoplasmic reticulum	0.08	Receptor expression-enhancing protein 2	Q8VCD6	1.08
26	GO:0005739 ~ mitochondrion	0.07	Cytochrome b-c1 complex subunit 2, mitochondrial	Q9DB77	5.31
27	GO:0003723 ~ RNA binding	0.05	Chromobox protein homolog 7	P60889	2.65

<https://doi.org/10.1371/journal.pone.0232981.t003>

metabolism. In addition, one of the transcripts matched and ERG-like transcription factor (known protooncogene) (Table 5).

Discussion

Here we show that the proper function of the Notch signaling pathway is required for arm regeneration in a brittle star. Pharmacological inhibition of the pathway with DAPT antagonist during the first 14 days of regeneration resulted in a significantly reduced overall length of the outgrowth and a smaller number of segments in the new arm. A similar effect of Notch pathway inhibition on regeneration was previously shown for sea urchin spines and podia.

Table 4. Down-regulated genes, unmapped by DAVID.

Trinity Transcript	Blast Hit Uniprot ID	Gene Name	Representative Annotation Term	Log ₂ Fold Change
TRINITY_DN113732_c3_g1_i1	P21328	RNA-directed DNA polymerase from mobile element jockey	GO:0003964 ~ RNA-directed DNA polymerase activity	-2.46
TRINITY_DN87639_c0_g1_i2	Q8I7P9	Retrovirus-related Pol polyprotein from transposon opus	GO:0003964 ~ RNA-directed DNA polymerase activity, GO:0015074 ~ DNA integration	-5.67
TRINITY_DN127189_c0_g1_i17	Q10126	Putative uncharacterized transposon-derived protein F52C9.6	NA	-2.75
TRINITY_DN154220_c1_g1_i9	Q95SX7	Probable RNA-directed DNA polymerase from transposon BS	GO:0003964 ~ RNA-directed DNA polymerase	-2.09
TRINITY_DN82736_c0_g1_i1	P14381	Transposon TX1 uncharacterized 149 kDa protein	NA	-5.95
TRINITY_DN168317_c0_g1_i3	P08548	LINE-1 reverse transcriptase homolog	GO:0003964 ~ RNA-directed DNA polymerase activity	-2.60
TRINITY_DN164170_c2_g2_i1	P10394	Retrovirus-related Pol polyprotein from transposon 412	GO:0003964 ~ RNA-directed DNA polymerase activity, GO:0015074 ~ DNA integration	-3.85
TRINITY_DN138975_c0_g1_i8	Q9PVW8	Rhamnose-binding lectin	GO:0030246 ~ carbohydrate binding	-3.96
TRINITY_DN159770_c4_g1_i1	P06027	Echinoidin	GO:0030246 ~ carbohydrate binding	-4.95
TRINITY_DN100482_c2_g1_i8	A8V0B3	Neuromacin	GO:0006952 ~ defense response	-5.04
TRINITY_DN141895_c2_g1_i5	Q9U8W7	Techylectin-5B	GO:0030246 ~ carbohydrate binding, GO:0098609 ~ cell-cell adhesion	-3.16
TRINITY_DN111423_c2_g1_i4	P38505	Calcium-binding protein	GO:0005509 ~ calcium ion binding	-3.70
TRINITY_DN150199_c1_g2_i1	Q2YEM9	Tripartite motif-containing protein 5	GO:0051607 ~ defense response to virus, GO:0006914 ~ autophagy	-4.42

<https://doi.org/10.1371/journal.pone.0232981.t004>

Treatment of DAPT resulted in a dosage-dependent reduction of regrowth of those structures post-amputation [20]. This suggests that the involvement of Notch signaling in the regeneration of body appendages is conserved among echinoderm classes.

The transcriptome-wide quantitative comparison of gene expression between the control individuals and the individuals with the inhibited Notch pathway provided us with an insight into the biological roles of the pathway in the brittle star arm regeneration. Our analyses show that the Notch signaling pathway directly or indirectly affects more than two thousand downstream genes.

Functional annotation of the genes that significantly changed their expression in response to the pathway perturbation suggested that Notch affects a wide array of biological phenomena in regeneration. Additionally, this work provides evidence suggesting that the activity of some of the mobile DNA elements (transposons) is, at least to some extent, regulated by Notch signaling.

First, multiple components of crucial cell signaling pathways changed their expression in both positive and negative ways in response to Notch pathway inhibition. This data indicates that individual pathways are not working in isolation during brittle star arm regeneration, but rather involved in a complex cross-coordination. This conclusion is consistent with previous studies that established the interaction of Notch signaling with other signaling pathway including, for example, the Bmp and Wnt pathways in the vertebrate heart development and repair [10], interaction between the Notch and Wnt signaling systems in *Drosophila* development and human cancers [37], and with the Wnt, BMP and Yap/Taz pathways in regulation of neuronal stem cells [38].

Second, a number of studies have previously demonstrated a crucial role of the extracellular matrix (ECM) remodeling in echinoderm regeneration [24, 39–41]. However, the upstream molecular mechanisms that initiate and coordinate these changes have heretofore not been

Table 5. Up-regulated genes, unmapped by DAVID.

Trinity Transcript	Blast Hit Uniprot ID	Gene Name	Representative Annotation Term	Log ₂ Fold Change
TRINITY_DN113902_c12_g1_i20	P34257	Transposable element Tc3 transposase	GO:0006313 ~ transposition, DNA-mediated	3.95
TRINITY_DN96178_c0_g1_i1	P04323	Retrovirus-related Pol polyprotein from transposon 17.6	GO:0003964 ~ RNA-directed DNA polymerase activity	2.84
TRINITY_DN155494_c1_g1_i1	Q9NBX4	Probable RNA-directed DNA polymerase from transposon X-element	GO:0003964 ~ RNA-directed DNA polymerase activity	5.33
TRINITY_DN147574_c9_g2_i2	Q95SX7	Probable RNA-directed DNA polymerase from transposon BS	GO:0003964 ~ RNA-directed DNA polymerase	6.69
TRINITY_DN116575_c4_g1_i14	O50655	Integrase/recombinase xerD homolog	GO:0044826 ~ viral genome integration into host DNA	4.46
TRINITY_DN163877_c0_g2_i2	Q09575	Uncharacterized protein K02A2.6	GO:0015074 ~ DNA integration	2.80
TRINITY_DN91925_c0_g1_i1	P46023	G-protein coupled receptor GRL101	GO:0007186 ~ G protein-coupled receptor signaling pathway	3.49
TRINITY_DN93460_c0_g1_i14	Q9I926	Fucolectin-6	GO:0045088 ~ regulation of innate immune response	5.33
TRINITY_DN89036_c0_g1_i1	F7J220	Scavenger receptor cysteine-rich domain superfamily protein	GO:0045087 ~ innate immune response	2.60
TRINITY_DN163643_c0_g1_i11	Q53B88	Nucleotide-binding oligomerization domain-containing protein 2	GO:0045087 ~ innate immune response	4.20
TRINITY_DN87261_c0_g1_i1	Q9GV77	Extracellular matrix protein 3	GO:0007155 ~ cell adhesion	7.73
TRINITY_DN136305_c0_g1_i9	P81721	Vesicular acetylcholine transporter	GO:0006836 ~ neurotransmitter transport	3.28
TRINITY_DN160426_c0_g1_i8	Q9U518	L-asparaginase	GO:0006520 ~ cellular amino acid metabolic process	2.17
TRINITY_DN111554_c1_g1_i4	A7X3X8	C-type lectin lectoxin-Enh5	GO:0030246 ~ carbohydrate binding	6.7
TRINITY_DN88709_c0_g1_i1	Q01414	Transcriptional regulator ERG homolog	GO:0003700 ~ DNA-binding transcription factor activity	5.90
TRINITY_DN105897_c0_g3_i1	Q8TQD0	Macrodomain-containing protein MA_1614	NA	5.62
TRINITY_DN91758_c0_g1_i1	C0HL13	Low-density lipoprotein receptor-related protein 2	GO:0006898 ~ receptor-mediated endocytosis	5.20

<https://doi.org/10.1371/journal.pone.0232981.t005>

described. Our data here suggests that in brittle star arm regeneration, Notch signaling is involved in both positive and negative regulation of different aspects of ECM composition and cell-ECM interaction, including cell migration.

Third, perturbation of Notch signalling results in downregulation of innate immune pathways, suggesting that they are positively regulated by the pathway in regenerating tissues. These include lectins, antiviral response, and phagocytosis. This elevated immune response might represent a reaction to the invasion of pathogens and the accumulation of damaged or necrotic cells at the site of autonomy. Alternatively, molecular components of the innate immune response are also known to function as key modulators of regeneration, including wound healing and cell division [42]. For example, innate immune mechanisms are known to facilitate changes in epigenetic states and activate mechanisms required for nuclear reprogramming and cell dedifferentiation [43].

Fourth, the Notch signaling performs its classical functions in regulating cell proliferation, survival, programmed cell death, and differentiation in brittle star arm regeneration. All these cell events are prominently involved in regeneration in *O. brevispinum* (Mashanov et al., in preparation), and in other echinoderms [44].

Fifth, the Notch pathway controls some of the cellular housekeeping functions, such as regulation of the endoplasmic reticulum, ion balance, ribosomes, RNA processing, and mitochondrial function.

Sixth, Notch affects transcriptional activity (both positively and negatively) of mobile genetic elements (RNA and DNA transposons). Transposons, especially RNA transposons, are known to be active not only in the germ line, but also in somatic cells. Transposons affect the host cell gene expression via various mechanisms, including 1) providing promoter and enhancer sites that change the expression of the host genes, 2) creating splice and polyadenylation sites, and 3) through RNA interference [45]. Although, in some cases, transposon activation is known to cause genetic disorders and autoimmune reactions [45], they do also play important “positive” roles in adult and developing tissues. For example, in mammalian neurogenesis retrotransposition activity of LINE-1 elements contributes to neuronal diversity [46, 47]. We have also recently shown that retrotransposons are differentially expressed in the sea cucumber neural regeneration. In response to injury, some of the retroelements increased their levels of expression, but there were others that were suppressed. The cells with activated retroelement activity remained alive and contributed to the newly regenerated tissues [48, 49]. We have hypothesized that mobile DNA plays a role in post-traumatic regeneration in echinoderms. The host molecular mechanisms that differentially regulate the transcriptional activity of mobile genetic elements are largely unknown. This work provides evidence that the activity of mobile DNA is controlled by a cell signaling pathway. Our data also provide further mechanistic insight into how Notch can positively regulated expression of retroelements. One of the genes repressed by active Notch signaling is deoxynucleoside triphosphate triphosphohydrolase SAMHD1 (Table 3), an antiviral protein that is also known to inhibit endogenous retroelements such as LINE-1 [50]. Therefore, in the brittle star arm regeneration, the Notch pathway can activate retrotransposons through the double negative regulation mechanism.

Our data also provide an insight into how the Notch signaling, once activated, might sustain its function in the brittle star arm regeneration. One of the genes that we found to be suppressed by the pathway is a homolog of Neuralized1, which is an antagonist of the Notch pathway [51].

We fully understand advantages and limitations of the whole-transcriptome RNA-seq gene expression analysis approach implemented in this study. On the one hand, this strategy provides us with an insight into an array of direct and indirect targets of the Notch pathway, including discovery of new roles for genes in regeneration, such transposons. On the other hand, this approach lacks the resolution to distinguish between the immediate targets of the pathways and those that may be several levels farther down the gene regulatory network hierarchy. Nevertheless, the present study yields a valuable resource in the form of a catalog of Notch-affected genes involved in regeneration. Ongoing and future functional genomics work will further unravel the details of the functional relationships between the individual genetic components and their specific functional involvement in post-traumatic tissue formation.

Conclusions

- The activity of the Notch signaling pathway is required for proper post-autotomy regeneration of the brittle star arm. Inhibition of the pathway results in a significant reduction of the outgrowth rate.
- There is evidence of an extensive cross-talk between the Notch pathway and other signaling pathways in the cell.

- Inhibition of the Notch pathway affects a wide range of cellular and molecular processes in the regenerating tissues, including:
 - composition and remodeling of the extracellular matrix
 - cell adhesion and migration
 - innate immune response
 - cell proliferation, survival, differentiation, and programmed cell death
 - “housekeeping functions” (functions of the endoplasmic reticulum, ribosomes, mitochondria, RNA processing, ion balance).
- The Notch pathway directly or indirectly regulates (positively or negatively) the activity of several RNA and DNA transposable elements.
- A possible mechanism by which Notch sustains its activity in the regenerating tissues is suppression of Neuralized1.

Methods

Animal maintenance and pharmacological treatment

Adult individuals of the brittle star *Ophioderma brevispina* (Say, 1825) were purchased from the Marine Biological Laboratory (Woods Hole, MA) and were allowed to acclimate overnight in aerated sea water before being subjected to experimental procedures.

The DAPT reagent, N-[N-(3,5-Difluorophenacetyl)-L-alanyl]-S-phenylglycine t-butyl ester, was purchased from Sigma-Aldrich (catalog number D5942) and dissolved in DMSO (Dimethyl sulfoxide) to make a 20 mM stock solution.

The animals were divided into two cohorts (5 animals in each)—the DAPT treatment group and the control group. The DAPT treatment cohort was continuously exposed to 3 μ M DAPT prepared by diluting the stock solution in filtered seawater. The control group was exposed to the matching concentration of DMSO (vehicle). The animals were kept in glass vials submerged in 200 ml of the DAPT or DMSO solution, respectively. The solutions were changed daily.

The treatments started when the animals still have intact arms; then, after 24 hours, the arms were autotomized as described below and the treatments continued until 14 days post-autotomy.

In each individual, all five arms were autotomized by squeezing a single arm segment with a fine forceps. Since the rate of regeneration in serpent stars is known to vary with the position of the autotomy plane along the proximodistal axis of the arm [25], we kept the injury paradigm consistent by autotomizing all arms at the level of the 15th segment (counting from the disk).

On day 14 post-autotomy, three of the five arms of each animal were pooled and used for total RNA extraction. The two remaining arms from each individual were processed for histological analysis.

Histology and image analysis

Tissue samples were fixed overnight in 4% paraformaldehyde prepared in 0.01M PBS (pH 7.4) at 4°C. Fixed tissues were washed in PBS, decalcified in 10% EDTA, cryoprotected in graded sucrose solutions, and embedded in the Tissue-Tek OCT medium (Sakura). Serial longitudinal

sections (10 μm thick) were cut with a Leica CM1860 cryostat, collected on gelatin-covered slides, and incubated at 42°C overnight. They were then stained with Hematoxylin and Eosin and mounted in the DPX Medium (Electron Microscopy Sciences). The sections were photographed using an Olympus BX60 compound microscope equipped with a SPOT RT camera. The length of the regenerating arm was measured in six animals from each treatment group using the Fiji/ImageJ software [52, 53] in calibrated micrographs. The means between the two conditions were compared using Student's T-test in R [54].

Total RNA extraction

The tissue samples for RNA extraction included the most distal segment of the stump and the entire outgrowth (regenerate). The samples from three arms of each individual were pooled together and quickly homogenized in 500 μl of ice-cold TRI reagent (Sigma-Aldrich, 93289) using a disposable Micro Tissue Homogenizer (Kimble, K7496250030). The homogenized samples were briefly vortexed, an additional 500 μl of the TRI reagent were added to each tube, and the subsequent steps of RNA purification were performed as directed by the manufacturer's protocol.

Sequencing

Illumina HiSeq. Three total RNA samples from DAPT-treated individuals (each sample representing a different individual) and three samples from control individuals (DMSO-treated) were used for sequencing on the Illumina HiSeq 2000/2500 platform. The libraries were barcoded, pooled, and sequenced in a single flow cell in the Rapid Mode (2 \times 100 bp). These reads were used both for the *de novo* transcriptome assembly and for gene expression analysis, as reads corresponding to each individual library could be identified and analyzed separately.

Illumina MiSeq. To facilitate the *de novo* assembly, we also prepared the following single combined sample to maximize the representation of expressed genes in the assembled reference transcriptome. Total RNA was extracted as above from intact animals and from untreated regenerating individuals on days 1, 3, 5, 18, and 30 post-autotomy. Each condition was represented by seven individuals. These 42 RNA samples (6 conditions \times 7 individuals) were mixed in equimolar quantities and sequenced on the Illumina MiSeq platform (2 \times 250 bp). The final stages of library preparation and sequencing were outsourced to the Duke Center for Genomic and Computational Biology. The raw sequencing reads were deposited at the NCBI Sequence Read Archive (SRA) under the accession number GSE142391 (<https://www.ncbi.nlm.nih.gov/geo/query/acc.cgi?acc=GSE142391>).

De novo transcriptome assembly and quality assessment

The code used for the transcriptome assembly and subsequent RNAseq data analysis can be found in the accompanying additional file (S2 File). The raw Illumina reads were trimmed with Trim Galore [55] to remove adapter sequences and low-quality bases at the 3'-end (with the base quality < 20). If a cleaned read was shorter than 20 nt, the entire read pair was discarded. This procedure yielded 17,318,775 MiSeq read pairs (combined library with pooled samples from different arm regeneration stages) with the read length ranging between 20–250 nt. Individual HiSeq libraries representing control and DAPT-treated individuals contained 34,676,875 \pm 5,960,462 (mean \pm standard deviation) read pairs with sequence length ranging between 20–100 nt. The total number of cleaned HiSeq read pairs was 832,245,006. All cleaned Illumina reads, from both the MiSeq and HiSeq technologies, were pooled and assembled with Trinity [26, 27] with the minimum reported contig length of 150 nt. The assembled

transcriptome is available at the NCBI Gene Expression Omnibus (GEO) database (accession number GSE142391). The quality of the assembly was assessed by running several tests. First, to assess the representation of reads in the *de novo* transcriptome, we mapped all quality trimmed Illumina reads back to the assembled contigs using Bowtie 2 (Version 2.1.0) [28]. Second, we determined the number of completely or almost completely (>80% of the length) assembled protein-coding transcripts by comparing our contigs to the reference proteome of the sea urchin *S. purpuratus* [29]. Third, the completeness of protein-coding gene representation in the transcriptome was assessed with BUSCO (v3.0.2) [30] run in the “transcriptome mode” against the evolutionary conserved metazoan gene set (metazoa_odb9, creation date: 2016-02-13, number of species: 65, number of BUSCOs: 978).

Identification of the main components of the Notch signaling pathway

To identify the main components of the Notch signaling pathway in the transcriptome of *O. brevispina*, we performed BLAST analysis (tblastn, E-value cutoff of $1e-5$; [56]) using Notch-related genes from the published transcriptomes of *H. glaberrima* [17] and *S. purpuratus* [5], keeping all hits. Each transcript identified this way was considered a putative Notch-related gene. We then used the NCBI’s conserved domain database (CDD; [57]) to search for conserved domains that are categorize the target genes, including the Notch receptor, ligands (Delta and Serrate), the transcriptional regulator RBPJ, two Notch target genes of the Hes family (orthologous to HES-1 and HES-4), and the Notch signaling modulator Numb.

Differential gene expression analysis

The cleaned reads from each of the six Illumina HiSeq libraries representing the control and DAPT-treated animals were aligned back to the assembled contigs using the Salmon tool (version v0.13.1) [33] with the *-dumpEq*, *-validateMappings*, and *-hardFilter* options. We then used Corset (version 1.08) [32] to mitigate the redundancy issue inherent to *de novo* transcriptome assemblies. Corset clusters isoforms into “genes” based on the proportion of shared reads and expression patterns and thus outputs gene-level counts.

Quantitative gene expression analysis was performed using the DESeq R package [34]. To optimize memory usage, the raw count matrix was pre-filtered by only keeping rows that contained 10 reads or more. After normalizing the data and fitting the model, the independent hypothesis weighting approach for *p*-value adjustment implemented in the IHW R package [58] was applied to optimize the statistical power of the analysis. To improve fold change estimates for the gene expression data, a DESeq2 log2 fold change shrinking algorithm was applied. It uses information from all genes to improve the estimates for genes expressed at low levels with high dispersion values but does not change the total number of genes that are identified as differentially expressed [34]. Genes were considered differentially expressed if their adjusted *p*-value was below 0.05 and the fold change in expression level exceeded 1.5 in either direction. The gene expression data were submitted to the GEO database (accession number GSE142391).

Functional annotation of differentially expressed genes was performed using DAVID (Database for Annotation, Visualization, and Integrated Discovery) [35], which was accessed from within R interface using the RDAVIDWebService package [36]. To prepare data for DAVID, we annotated the Trinity transcripts representing all Corset clusters by matching them to the Uniprot database using BLASTX with the cutoff e-value threshold of 10^{-5} . The resulting list of Uniprot accession IDs was used as the background gene set for DAVID. The up-regulated and down-regulated genes were annotated in the similar manner before being imported into DAVID. For functional annotation, we set the following annotation categories:

“GOTERM_BP_ALL”, “GOTERM_MF_ALL”, “GOTERM_CC_ALL”, “KEGG_PATHWAY”, “BIOCARTA”, and “PFAM”. DAVID cluster reports were parsed and analyzed using a custom R function ([S2 File](#)).

Supporting information

S1 File. General feature format file. This file contains a GFF3 file which includes the sequence data and annotation of the main components of the Notch signaling pathway in *O. brevispina*. (GFF)

S2 File. R markdown document. This file contains all shell and R code used for transcriptome assembly and statistical analysis. The file can be opened in RStudio or any text editor. (RMD)

Author Contributions

Conceptualization: Vladimir Mashanov, Olga Zueva.

Data curation: Jacob Ferrier, Robert Reid, Daniel Janies.

Formal analysis: Vladimir Mashanov, Jennifer Akiona, Maleana Khoury, Robert Reid.

Funding acquisition: Vladimir Mashanov, Daniel Janies.

Investigation: Vladimir Mashanov, Jennifer Akiona, Maleana Khoury, Robert Reid, Denis Jacob Machado, Olga Zueva.

Methodology: Vladimir Mashanov, Jacob Ferrier, Robert Reid, Denis Jacob Machado, Olga Zueva.

Project administration: Vladimir Mashanov, Daniel Janies.

Resources: Daniel Janies.

Software: Vladimir Mashanov, Robert Reid, Denis Jacob Machado.

Supervision: Vladimir Mashanov, Daniel Janies.

Validation: Vladimir Mashanov, Denis Jacob Machado.

Visualization: Vladimir Mashanov.

Writing – original draft: Vladimir Mashanov, Denis Jacob Machado.

Writing – review & editing: Vladimir Mashanov, Jennifer Akiona, Denis Jacob Machado, Daniel Janies.

References

1. Gazave E, Lapébie P, Richards GS, Brunet F, Ereskovsky AV, Degnan BM, et al. Origin and evolution of the Notch signaling pathway: an overview from eukaryotic genomes. *BMC Evol Biol.* 2009; 9:249. <https://doi.org/10.1186/1471-2148-9-249> PMID: 19825158
2. Marlow H, Roettinger E, Boekhout M, Martindale MQ. Functional roles of Notch signaling in the cnidarian *Nematostella vectensis*. *Dev Biol.* 2012; 362(2):295–308. <https://doi.org/10.1016/j.ydbio.2011.11.012> PMID: 22155407
3. Layden MJ, Martindale MQ. Non-canonical Notch signaling represents an ancestral mechanism to regulate neural differentiation. *EvoDevo.* 2014; 5:30. <https://doi.org/10.1186/2041-9139-5-30> PMID: 25705370
4. Favaro MB, López SL. Notch signaling in the division of germ layers in bilaterian embryos. *Mech Dev.* 2018; 154:122–144. <https://doi.org/10.1016/j.mod.2018.06.005> PMID: 29940277

5. Walton KD, Croce JC, Glenn TD, Wu SY, McClay DR. Genomics and expression profiles of the Hedgehog and Notch signaling pathways in sea urchin development. *Dev Biol.* 2006; 300(1):153–164. <https://doi.org/10.1016/j.ydbio.2006.08.064> PMID: 17067570
6. Erkenbrack EM. Notch-mediated lateral inhibition is an evolutionarily conserved mechanism patterning the ectoderm in echinoids. *Dev Genes Evol.* 2018; 228(1):1–11. <https://doi.org/10.1007/s00427-017-0599-y> PMID: 29249002
7. Hinman VF, Burke RD. Embryonic neurogenesis in echinoderms. *Wiley Interdiscip Rev Dev Biol.* 2018; 7(4):e316. <https://doi.org/10.1002/wdev.316> PMID: 29470839
8. Lloyd-Lewis B, Mourikis P, Fre S. Notch signaling: sensor and instructor of the microenvironment to coordinate cell fate and organ morphogenesis. *Curr Opin Cell Biol.* 2019; 61:16–23. <https://doi.org/10.1016/j.ceb.2019.06.003> PMID: 31323467
9. Miele L. Notch signaling. *Clinical Cancer Research.* 2006; 12(4):1074–1079. <https://doi.org/10.1158/1078-0432.CCR-05-2570> PMID: 16489059
10. MacGrogan D, Münch J, de la Pompa JL. Notch and interacting signaling pathways in cardiac development, disease, and regeneration. *Nat Rev Cardiol.* 2018; 15(11):685–704. <https://doi.org/10.1038/s41569-018-0100-2> PMID: 30287945
11. Münder S, Tischer S, Grundhuber M, Büchels N, Bruckmeier N, Eckert S, et al. Notch-signaling is required for head regeneration and tentacle patterning in *Hydra*. *Dev Biol.* 2013; 383(1):146–57. <https://doi.org/10.1016/j.ydbio.2013.08.022> PMID: 24012879
12. Nakamura K, Chiba C. Evidence for Notch signaling involvement in retinal regeneration of adult newt. *Brain Res.* 2007; 1136(1):28–42. <https://doi.org/10.1016/j.brainres.2006.12.032> PMID: 17217933
13. Zhao L, Borikova AL, Ben-Yair R, Guner-Ataman B, MacRae CA, Lee RT, et al. Notch signaling regulates cardiomyocyte proliferation during zebrafish heart regeneration. *Proc Natl Acad Sci U S A.* 2014; 111(4):1403–8. <https://doi.org/10.1073/pnas.1311705111> PMID: 24474765
14. Wenemoser D, Lapan SW, Wilkinson AW, Bell GW, Reddien PW. A molecular wound response program associated with regeneration initiation in planarians. *Genes Dev.* 2012; 26(9):988–1002. <https://doi.org/10.1101/gad.187377.112> PMID: 22549959
15. Ben Khadra Y, Sugni M, Ferrario C, Bonasoro F, Oliveri P, Martinez P, et al. Regeneration in Stellate Echinoderms: Crinoidea, Asteroidea and Ophiuroidea. *Results Probl Cell Differ.* 2018; 65:285–320. https://doi.org/10.1007/978-3-319-92486-1_14 PMID: 30083925
16. García-Arrarás JE, Lázaro-Peña MI, Díaz-Balzac CA. Holothurians as a Model System to Study Regeneration. *Results Probl Cell Differ.* 2018; 65:255–283. https://doi.org/10.1007/978-3-319-92486-1_13 PMID: 30083924
17. Mashanov VS, Zueva OR, García-Arrarás JE. Transcriptomic changes during regeneration of the central nervous system in an echinoderm. *BMC Genomics.* 2014; 15(1):357. <https://doi.org/10.1186/1471-2164-15-357> PMID: 24886271
18. Mellott DO, Thisdelle J, Burke RD. Notch signaling patterns neurogenic ectoderm and regulates the asymmetric division of neural progenitors in sea urchin embryos. *Development.* 2017; 144(19):3602–3611. <https://doi.org/10.1242/dev.151720> PMID: 28851710
19. Foster S, Teo YV, Neretti N, Oulhen N, Wessel GM. Single cell RNA-seq in the sea urchin embryo show marked cell-type specificity in the Delta/Notch pathway. *Mol Reprod Dev.* 2019; 86(8):931–934. <https://doi.org/10.1002/mrd.23181> PMID: 31199038
20. Reinardy HC, Emerson CE, Manley JM, Bodnar AG. Tissue regeneration and biomineralization in sea urchins: role of Notch signaling and presence of stem cell markers. *PLoS One.* 2015; 10(8):e0133860. <https://doi.org/10.1371/journal.pone.0133860> PMID: 26267358
21. Byrne M. Ophiuroidea. In: Harrison FW, Chia FS, editors. *Microscopic Anatomy of Invertebrates.* vol. 14. New York: Wiley-Liss; 1994. p. 247–343.
22. Zueva O, Khoury M, Heinzeller T, Mashanova D, Mashanov V. The complex simplicity of the brittle star nervous system. *Front Zool.* 2018; 15:1. <https://doi.org/10.1186/s12983-017-0247-4> PMID: 29434647
23. Czarkwiani A, Dylus DV, Oliveri P. Expression of skeletogenic genes during arm regeneration in the brittle star *Amphiura filiformis*. *Gene Expr Patterns.* 2013; 13(8):464–72. <https://doi.org/10.1016/j.gep.2013.09.002> PMID: 24051028
24. Czarkwiani A, Ferrario C, Dylus DV, Sugni M, Oliveri P. Skeletal regeneration in the brittle star *Amphiura filiformis*. *Front Zool.* 2016; 13:18. <https://doi.org/10.1186/s12983-016-0149-x> PMID: 27110269
25. Dupont S, Thorndyke MC. Growth or differentiation? Adaptive regeneration in the brittlestar *Amphiura filiformis*. *Journal of Experimental Biology.* 2006; 209(19):3873–3881. <https://doi.org/10.1242/jeb.02445> PMID: 16985203

26. Grabherr MG, Haas BJ, Yassour M, Levin JZ, Thompson DA, Amit I, et al. Full-length transcriptome assembly from RNA-Seq data without a reference genome. *Nat Biotechnol.* 2011; 29(7):644–652. <https://doi.org/10.1038/nbt.1883> PMID: 21572440
27. Haas BJ, Papanicolaou A, Yassour M, Grabherr M, Blood PD, Bowden J, et al. *De novo* transcript sequence reconstruction from RNA-seq using the Trinity platform for reference generation and analysis. *Nat Protoc.* 2013; 8(8):1494–1512. <https://doi.org/10.1038/nprot.2013.084> PMID: 23845962
28. Langmead B, Salzberg SL. Fast gapped-read alignment with Bowtie 2. *Nat Methods.* 2012; 9(4):357–359. <https://doi.org/10.1038/nmeth.1923> PMID: 22388286
29. The NCBI collection of predicted proteins of the sea urchin *Strongylocentrotus purpuratus*. Available from: ftp://ftp.ncbi.nih.gov/genomes/Strongylocentrotus_purpuratus/protein/.
30. Simão FA, Waterhouse RM, Ioannidis P, Kriventseva EV, Zdobnov EM. BUSCO: assessing genome assembly and annotation completeness with single-copy orthologs. *Bioinformatics.* 2015; 31(19):3210–3212. <https://doi.org/10.1093/bioinformatics/btv351> PMID: 26059717
31. Vijay N, Poelstra JW, Künstner A, Wolf JBW. Challenges and strategies in transcriptome assembly and differential gene expression quantification. A comprehensive in silico assessment of RNA-seq experiments. *Molecular Ecology.* 2013; 22(3):620–634. <https://doi.org/10.1111/mec.12014> PMID: 22998089
32. Davidson NM, Oshlack A. Corset: enabling differential gene expression analysis for *de novo* assembled transcriptomes. *Genome Biology.* 2014; 15(7):410. <https://doi.org/10.1186/s13059-014-0410-6> PMID: 25063469
33. Patro R, Duggal G, Love MI, Irizarry RA, Kingsford C. Salmon provides fast and bias-aware quantification of transcript expression. *Nature Methods.* 2017; 14(4):417. <https://doi.org/10.1038/nmeth.4197> PMID: 28263959
34. Love MI, Huber W, Anders S. Moderated estimation of fold change and dispersion for RNA-seq data with DESeq2. *Genome Biology.* 2014; 15(12):550. <https://doi.org/10.1186/s13059-014-0550-8> PMID: 25516281
35. Huang DW, Sherman BT, Lempicki RA. Systematic and integrative analysis of large gene lists using DAVID bioinformatics resources. *Nature Protocols.* 2009; 4(1):44–57. <https://doi.org/10.1038/nprot.2008.211>
36. Fresno C, Fernández EA. RDAVIDWebService: a versatile R interface to DAVID. *Bioinformatics.* 2013; 29(21):2810–2811. <https://doi.org/10.1093/bioinformatics/btt487> PMID: 23958726
37. Hayward P, Brennan K, Sanders P, Balayo T, DasGupta R, Perrimon N, et al. Notch modulates Wnt signaling by associating with Armadillo/ β -catenin and regulating its transcriptional activity. *Development.* 2005; 132(8):1819–1830. <https://doi.org/10.1242/dev.01724> PMID: 15772135
38. Zhang R, Engler A, Taylor V. Notch: an interactive player in neurogenesis and disease. *Cell Tissue Res.* 2018; 371(1):73–89. <https://doi.org/10.1007/s00441-017-2641-9> PMID: 28620760
39. Quiñones JL, Rosa R, Ruiz DL, García-Arrarás JE. Extracellular matrix remodeling and metalloproteinase involvement during intestine regeneration in the sea cucumber *Holothuria glaberrima*. *Dev Biol.* 2002; 250(1):181–97. <https://doi.org/10.1006/dbio.2002.0778> PMID: 12297105
40. Lamash NE, Dolmatov IY. Proteases from the regenerating gut of the holothurian *Eupentacta fraudatrix*. *PLoS One.* 2013; 8(3):e58433. <https://doi.org/10.1371/journal.pone.0058433> PMID: 23505505
41. Vázquez-Vélez GE, Rodríguez-Molina JF, Quiñones-Frías MC, Pagán M, García-Arrarás JE. A Proteoglycan-Like Molecule Offers Insights Into Ground Substance Changes During Holothurian Intestinal Regeneration. *J Histochem Cytochem.* 2016; 64(6):381–93. <https://doi.org/10.1369/0022155416645781> PMID: 27126824
42. Gao L, Han Y, Deng H, Hu W, Zhen H, Li N, et al. The role of a novel C-type lectin-like protein from planarian in innate immunity and regeneration. *Dev Comp Immunol.* 2017; 67:413–426. <https://doi.org/10.1016/j.dci.2016.08.010> PMID: 27565408
43. Mescher AL, Neff AW, King MW. Inflammation and immunity in organ regeneration. *Dev Comp Immunol.* 2017; 66:98–110. <https://doi.org/10.1016/j.dci.2016.02.015> PMID: 26891614
44. García-Arrarás JE, Lázaro-Peña MI, Díaz-Balzac CA. Holothurians as a Model System to Study Regeneration. *Res Probl Cell Differ.* 2018; 65:255–283. https://doi.org/10.1007/978-3-319-92486-1_13
45. Suntsova M, Garazha A, Ivanova A, Kaminsky D, Zhavoronkov A, Buzdin A. Molecular functions of human endogenous retroviruses in health and disease. *Cell Mol Life Sci.* 2015; 72(19):3653–75. <https://doi.org/10.1007/s00018-015-1947-6> PMID: 26082181
46. Muotri AR, Chu VT, Marchetto MCN, Deng W, Moran JV, Gage FH. Somatic mosaicism in neuronal precursor cells mediated by L1 retrotransposition. *Nature.* 2005; 435(7044):903–10. <https://doi.org/10.1038/nature03663> PMID: 15959507
47. Suarez NA, Macia A, Muotri AR. LINE-1 retrotransposons in healthy and diseased human brain. *Dev Neurobiol.* 2018; 78(5):434–455. <https://doi.org/10.1002/dneu.22567> PMID: 29239145

48. Mashanov VS, Zueva OR, García-Arrarás JE. Posttraumatic regeneration involves differential expression of long terminal repeat (LTR) retrotransposons. *Dev Dyn*. 2012; 241(10):1625–36. <https://doi.org/10.1002/dvdy.23844> PMID: 22911496
49. Mashanov VS, Zueva OR, García-Arrarás JE. Retrotransposons in animal regeneration: Overlooked components of the regenerative machinery? *Mob Genet Elements*. 2012; 2(5):244–247. <https://doi.org/10.4161/mge.22644> PMID: 23550104
50. Herrmann A, Wittmann S, Thomas D, Shepard CN, Kim B, Ferreirós N, et al. The SAMHD1-mediated block of LINE-1 retroelements is regulated by phosphorylation. *Mob DNA*. 2018; 9:11. <https://doi.org/10.1186/s13100-018-0116-5> PMID: 29610582
51. Teider N, Scott DK, Neiss A, Weeraratne SD, Amani VM, Wang Y, et al. Neuralized1 causes apoptosis and downregulates Notch target genes in medulloblastoma. *Neuro Oncol*. 2010; 12(12):1244–56. <https://doi.org/10.1093/neuonc/noq091> PMID: 20847082
52. Schindelin J, Arganda-Carreras I, Frise E, Kaynig V, Longair M, Pietzsch T, et al. Fiji: an open-source platform for biological-image analysis. *Nat Methods*. 2012; 9(7):676–682. <https://doi.org/10.1038/nmeth.2019> PMID: 22743772
53. Rueden CT, Schindelin J, Hiner MC, DeZonia BE, Walter AE, Arena ET, et al. ImageJ2: ImageJ for the next generation of scientific image data. *BMC Bioinformatics*. 2017; 18(1):529. <https://doi.org/10.1186/s12859-017-1934-z> PMID: 29187165
54. R Core Team. R: A language and environment for Statistical computing; 2019. Available from: <https://www.R-project.org/>.
55. Trim Galore;. Available from: <https://github.com/FelixKrueger/TrimGalore>.
56. Altschul SF, Gish W, Miller W, Myers EW, Lipman DJ. Basic local alignment search tool. *Journal of Molecular Biology*. 1990; 215(3):403–410. [https://doi.org/10.1016/S0022-2836\(05\)80360-2](https://doi.org/10.1016/S0022-2836(05)80360-2) PMID: 2231712
57. Marchler-Bauer A, Derbyshire MK, Gonzales NR, Lu S, Chitsaz F, Geer LY, Geer RC, He J, Gwadz M, Hurwitz DI, et al. CDD: NCBI's conserved domain database. *Nucleic Acids Research*. 2014; 43(D1): D222–D226. <https://doi.org/10.1093/nar/gku1221> PMID: 25414356
58. Ignatiadis N, Klaus B, Zaugg JB, Huber W. Data-driven hypothesis weighting increases detection power in genome-scale multiple testing. *Nature Methods*. 2016; 13(7):577–580. <https://doi.org/10.1038/nmeth.3885> PMID: 27240256